A&A 401, 685–697 (2003)
DOI: 10.1051/0004-6361:20021901

Astronomy & Astrophysics

Dynamics of solar active regions

I. Photospheric and chromospheric oscillations observed with TRACE

K. Muglach⋆,⋆⋆

Astrophysikalisches Institut Potsdam, Telegrafenberg, 14473 Potsdam, Germany

Received 17 July 2002 / Accepted 23 December 2002

Abstract. I present results of an international joint observing campaign, which was carried out in September 1999 and 2000, to study the oscillatory behaviour of active regions (ARs). In this contribution I will concentrate on oscillations in the higher layers of the solar atmosphere as observed with the UV filters of the Transition Region and Coronal Explorer (TRACE). I present the distribution of oscillatory power of two extended active regions. I find a number of well–known chromospheric dynamic phenomena such as running penumbral waves, enhanced 5 min power in the plage and network regions and additional 3 min power in the internetwork. In addition, I find that the 3 min power in the surroundings of the AR is decreased, an effect that has not been observed before. From the topology of the magnetic field I infer that this can be explained by an interaction of the acoustic wavefield with the expanding magnetic field of the active region.

Key words. Sun: general – Sun: chromosphere – Sun: oscillations – Sun: activity

1. Introduction

In September 1999 and 2000 international joint observing campaigns were carried out[1] to study the oscillatory behaviour of active regions. The main goal of these campaigns was to obtain comprehensive information on the interaction of solar oscillations and the magnetic field on small spatial and short temporal scales. A range of height in the solar atmosphere, from the deep photosphere to the corona, was covered by a variety of instruments and observing techniques.

A number of aspects of active region oscillations have already been addressed in several investigations which resulted from these campaigns: umbral oscillations in the transition region (TR) and corona (Muglach & O'Shea 2001; O'Shea et al. 2002a,b), intensity variations around sunspots (Georgakilas et al. 2002) and photospheric oscillations in umbrae and pores (Balthasar et al. 2000a,b). Muglach (2002) presents preliminary results of this work.

In this contribution I will concentrate on oscillations in the high photosphere and low chromosphere as observed with the Transition Region and Coronal Explorer (TRACE, Handy et al. 1999). I have studied the spatial distribution of oscillatory power in extended active regions (ARs) that contain sunspots, surrounding plage and patches of quiet sun with network and internetwork.

⋆ e-mail: muglach@solphys.nrl.navy.mil
⋆⋆ *Present address*: Artep, Inc., Naval Research Laboratory, 4555 Overlook Ave. SW, Washington, DC 20375, USA.
[1] JOP097, see
http://sohowww.nascom.nasa.gov/soc/JOPs/jop097.txt

TRACE is a filtergraph instrument working in several EUV, UV and visible band–passes. The broad–band filters of TRACE provide a very clean intensity diagnostic that is not contaminated by crosstalk from velocity signals which might be the case for filtergrams like Ca II K or Hα. In its near–Earth orbit TRACE produces image sequences that are free of atmospheric disturbances. They can cover considerable duration, but are still limited by the time–scale of evolution of the solar structures if one actually wants to make use of the full spatial resolution of 1″. Also, the spacecraft passes through the Earth's radiation belts which limits long–duration uninterrupted sequences (see below).

The field of view (FOV) of the TRACE CCD of 512″×512″ covers a substantial fraction of the solar disk. However, the obtainable FOV is reduced due to a lack of solar rotation compensation and a limited telemetry which conflict with the need of high cadence and the demand for observations in several filters. On–board data compression can improve the situation, but it also increases the noise of the data (Aschwanden et al. 2000) as the compression algorithms are not lossless.

Earlier work on chromospheric dynamics deals with the sun outside active regions ("quiet sun"). An overview of this earlier ground–based work is given e.g. in Rutten & Uitenbroek (1991), while more recent work is described in Rutten (1999). The latest developments on sunspot oscillations are reviewed by Staude (1999) and Bogdan (2000).

Most earlier work was performed with spectrographs. They have the advantage of providing intensity as well as Doppler velocity to investigate the dynamics, but were limited

Table 1. Observational parameters: The first column gives the date of the data set and the second one the number of the active region. The images from 1999 contain two ARs, 8693 in the center of the FOV, which was the primary target of the campaign that day and 8699 at the top of the FOV. Column 3 gives the location of the center of the FOV away from disk center and Col. 4 the size of the FOV (as taken by the instrument). Column 5 gives the cadence of the images, calculated from the duration of the complete sequence divided by the number of images as indicated in Col. 6. Column 7 gives the Nyquist frequency, $\nu_{\rm Ny}$ in mHz, and Col. 8 the frequency resolution, $\Delta\nu$ in μHz. Column 9 finally indicates if white light images were taken interleaved with the UV observations.

date	AR	location [″ from center]	FOV [″]	cadence [s]	# of images	$\nu_{\rm Ny}$ mHz	$\Delta\nu$ μHz	comment
13/09/99	8693	–102, 93	128, 320	15.13	464	33.04	142.4	white light images
	8699							every 600 s
29/09/00	9172	–207, 93	192, 256	30.05	486	16.64	68.5	no white light images

to single slit positions on the disk and thus had very poor spatial coverage. In a few cases 2–d imaging was done (e.g. Kneer & v. Uexküll 1993) but they usually showed either spatially averaged power spectra or $k-\omega$ diagrams.

The first 2–d large–scale study of chromospheric AR dynamics comparable to this work was carried out by Braun et al. (1992). They used a 50 h sequence of full disk Ca II K images from the south pole. Interestingly, they found an enhancement of high frequency (3 min) acoustic power in the surroundings of ARs, while the actual locations of strong magnetic fields (sunspots) displayed a lack of power (at all frequencies) as has been known for a long time. Similar studies in Ca II K were later carried out by Toner & LaBonte (1993) and Thomas & Stanchfield (2000). They all found the same enhancements of high frequency power around the AR. Using lower temperature lines like Fe I (from ground) or Ni I (with MDI on SoHO) various groups searched for these features in the photosphere (Brown et al. 1992; Hindman & Brown 1998; Thomas & Stanchfield 2000; Donea et al. 2000; Jain 2001; Jain & Haber 2002). Power enhancements (also called power aureoles or halos) were present in 3 min velocity power maps. Their signature seems much weaker and patchier in the photosphere than in the Ca II K maps. No power enhancements were found in 5 min velocity maps and in photospheric continuum intensity maps. Hill et al. (2001) concluded that at least part of the patterns seen in acoustic power maps obtained from the ground can be due to the effect of seeing.

Recently, Krijger et al. (2001) carried out an analysis of TRACE data (similar to this one) restricted to the quiet sun, studying various network–internetwork issues. Note that the data sets of the two observing campaigns described in this article also included some true quiet sun (away from any ARs). As these results are in general compatible with the results of Krijger et al. (2001), they are not shown here.

This paper is structured in the following way: after this introduction a detailed description of the observations and the data reduction procedure are given in Sects. 2 and 3. Section 4 explains the results, which are discussed in Sect. 5. A summary and outlook are finally provided in Sect. 6.

2. Observations

I have selected two data sets, one taken in 1999 and one in 2000, see Tables 1 and 2 for details of the observational parameters. Note that a number of additional data sets have been analysed containing both various active regions and also quiet sun. The results of these datasets are in agreement with the results presented in this paper and can be found on my home page (`http://aipsoe.aip.de/~muglach/`).

TRACE observed in three of its UV filters which are centered at 1550 Å, 1600 Å and 1700 Å. An image was taken in each of these filters consecutively and the time to cycle through the three filters was about 15 s in 1999 and 30 s in 2000. The cadence as given in Table 1 is the time difference between two images of the same wavelength and thus the temporal resolution of the sequences. Note that in 1999 the observing sequence also included white light images, but these were taken every 10 min. Thus, the 1999 sequence does not have a completely regular cadence. The cadence given in Table 1 is the mean cadence calculated from the duration of the complete sequence and the number of images. Also, the complete sequence from 1999 was about 4 h, but after about 2 h TRACE moved though the Earth's radiation belts and apart from heavy contamination by high energetic particles the cadence also became quite irregular. Additionally, since the size of the FOV in E–W direction was rather narrow the spot moved out of the FOV due to solar rotation. For this reason I finally chose a 2 h sequence for the current analysis. Thus, the sequence of 1999 has a higher Nyquist frequency ($\nu_{\rm Ny}$ = 33.04 mHz) and less frequency resolution ($\Delta\nu$ = 142.4 μHz) compared to the sequence of 2000 ($\nu_{\rm Ny}$ = 16.64 mHz and $\Delta\nu$ = 68.5 μHz).

Also due to the different cadence the exposure times were changed between 1999 and 2000, being 5.6 s, 1 s, 2 s in 1999 and 9.7 s, 1.2 s, 3.4 s in 2000 for the three filters 1550 Å, 1600 Å, 1700 Å, respectively (see Table 2).

The 1700 Å filter covers mostly UV continuum, while the 1600 Å filter intensity is a combination of a continuum background, some small C I emission lines and some contribution of C IV. The 1550 Å filter is a rather narrowband filter centered at two strong emission lines of C IV (at 1548 Å and 1550 Å) (see Handy et al. 1999, Table 1 and Fig. 13).

According to the standard quiet sun VAL81 model (Vernazza et al. 1981) the disk center continuum intensity around 1700 Å originates from just below the temperature minimum region, 1600 Å from the temperature minimum and 1550 Å above the temperature minimum (which is located at h = 500 km). Of course, the 1550 Å filter includes the two

Table 2. Exposure times (in seconds) for the three filters (1550 Å, 1600 Å and 1700 Å) are given together with the date of the observations.

date	exp. time 1550 Å [s]	exp. time 1600 Å [s]	exp. time 1700 Å [s]
13/09/99	5.6	1.0	2.0
29/09/00	9.7	1.2	3.4

strong C IV lines which originate at transition region temperatures (log $T = 5.0$). Thus, the 1700 Å images are the "cleanest" diagnostic for the high photosphere/low chromosphere. Both 1600 Å and especially 1550 Å sample a combination of light from different heights and temperatures.

In the following sections I describe the details of the data reduction. Note that I do not use the standard SolarSoft data reduction procedures, as they are often not sufficient (the standard procedure would be to use the "trace_prep" routine, which uses certain standard values for the various steps described below).

3. Data reduction

3.1. Background subtraction

Dark exposures were taken on several days. These images show a diagonal light/dark pattern which changes in time and moves over the CCD. To calculate the dark offset this pattern could be successfully removed with a 2–d Fourier filter from each individual dark exposure. All dark images are then averaged to give the final dark correction applied to the actual images of the time sequence. This readout-pattern (which is electronic in its nature) is also present in the time sequence data. Due to the fact that the pattern moves over the CCD and the solar structures also move over the chip due to solar rotation this pattern introduces an oscillatory variation of intensities. Tests with using different darks (with and without the pattern removed) as well as using the standard dark (nearest temporal dark in the TRACE database provided with the TRACE software) confirm that the lowest temporal frequencies in our resulting intensity power spectra are most strongly influenced by this effect. Note that the pattern has a peak–to–peak value of about 4 DN/s and an rms of about 1.4 DN/s. Thus, areas that have low intensity levels will be influenced most (e.g. the sunspot umbra). In addition, Aschwanden et al. (2000) found a temperature dependence of the dark background and the noise level of the readout, which is an orbital effect. Checking for this effect, I indeed find a sinusoidal variation of the temperature of the CCD with a period of about 50 min. These changes also introduce a regular variation in the background and can create additional power peaks at the lowest frequencies.

3.2. Normalization to exposure time

The data are normalized to exposure time, which gives data numbers per second (DN s^{-1}). No absolute calibration of the data is applied.

3.3. Despiking

In its near–Earth high–inclination orbit TRACE passes regularly through the Earth's radiation belts whose high energetic particles produce high intensity pixels. To remove them I use the same routine as described in Aschwanden et al. (2000), which applies a temporal and spatial mean for comparison and substitutes the hot pixel (the same routine is also used to clean the dark images). The contamination with spikes is worst in the 1550 Å images as they have the longest exposure time. I carried out a second deep cleaning of the 1550 Å data. Still, the 1550 Å data contain some residual noise during the time of the passage which has to be considered with care in the results.

3.4. Filling in missing images

In some cases single images were missing in the sequence. Missing images were interpolated by using the average of the two neighbouring images (although in case of the data I selected for this article, no images were missing).

3.5. Flatfielding

Due to a long-term burn–in effect there is a large–scale decrease of sensitivity of the CCD from the edge to the center of the chip (see Handy et al. 1999). We take this into account by fitting a paraboloid to some quiet sun calibration data taken in September 1999 and 2000. Since no reliable flatfield images are available no pixel–to–pixel correction is applied. There seems to be no spatially repetitive pattern in the flatfield image shown in the instrument guide. Thus, I do not think the missing flatfield will introduce artificial peaks into the power spectra, although it will increase the overall noise.

3.6. Co–alignment

As we are interested in the temporal change of single pixels, we have to properly co–align the sequence of images so as not to mix temporal and spatial changes. This is done in a two step procedure.

3.6.1. Correction of differential solar rotation

First, we calculate the shift between the first and the last image of the sequence due to solar differential rotation (according to the equation of Howard et al. 1990). This is calculated for the central column of the image. A shearing of the images due to differential rotation is corrected. This amounts to a difference of 0.5 pixels between the equatorial and the northern-most part of the image over 1 h for the Sep. 2000 data.

3.6.2. Correction of image drift

As a second step we calculate the shift of the images by a two-dimensional cross-correlation of the image sequence. The resulting drift amounts to about 3 pixels in E–W and 3 pixels in N–S in 2000 and 1.5 pixels in E–W and 2 pixels in N–S in 1999. This reflects the drift in the pointing of the spacecraft

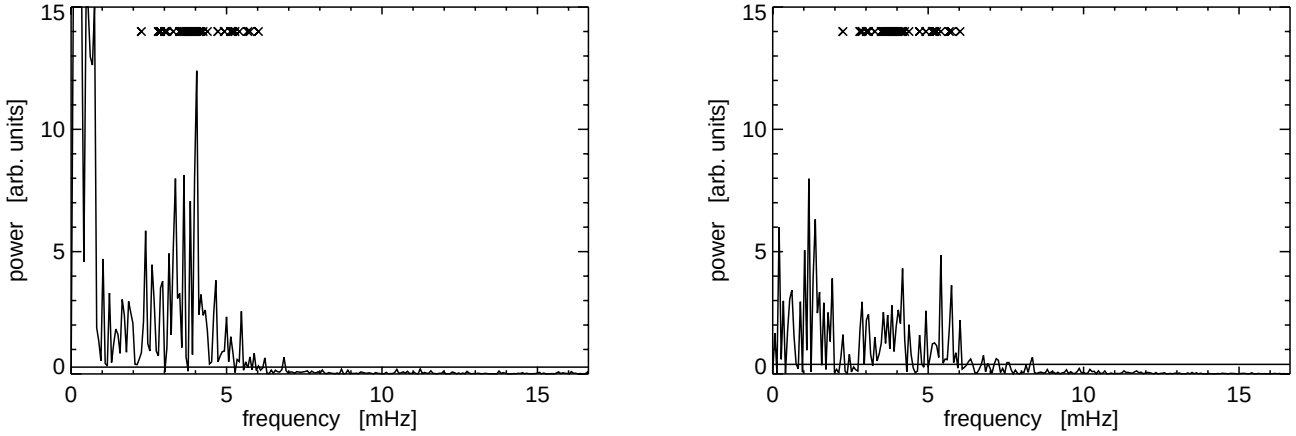

Fig. 1. Two examples of power spectra from a network (left) and an internetwork region (right). The horizontal line gives the 99% significance level calculated according to Groth. The crosses on top of the figures indicate the significant frequencies found by the randomisation test.

and shows an orbital variation (cf. Handy et al. 1999, Sect. 2.5). Note that there is an additional spatial offset between the filters of about 1 pixel that also displays an orbital variation. This has not been taken into account when displaying the final power maps.

The final time sequences can be viewed as movies, which can be found on my home page (`http://aipsoe.aip.de/~muglach/`). This can be used to check the quality of the co–alignment. Note that the co–alignment is calculated for the complete two-dimensional images. Thus, it represents the global drift of the images. Due to the evolution of the various solar structures one can still see some of them move within the FOV. For example the bright structures in the moat around the sunspot produce the radial streaks seen around the spot in the temporally averaged image of Fig. 2.

3.7. Power spectra

After this procedure one has a time sequence of intensity (DN s^{-1}) for each pixel of the image. Finally, I calculate power spectra using a Fast Fourier Transform (FFT), which includes a subtraction of the mean intensity and a 10% cosine apodisation. Note that the FFT requires equidistant time series, which is not strictly the case for the data of 1999 due to the interleaved white light images.

3.8. Statistical tests

Several components contribute to the power spectra: (i) oscillations, sinusoidal intensity variations which produce peaks in the power spectra and are the main topic of interest in this work. (ii) Non–oscillatory intensity variations that are still solar in their origin, e.g. short–term brightenings that propagate over the FOV along arcs (which are probably low–lying magnetic field structures) and that last for a few minutes (see UV movies on my home page or on the TRACE home page, `http://vestige.lmsal.com/TRACE/`). In the time domain these brightenings act like step functions and produce considerable power at all frequencies in the Fourier domain. The higher the formation height the more often they occur. They are especially frequent in the data of the 1550 Å filter and are a signature of transition region dynamics. Other possible sources of non-oscillatory power are convection and the evolution of the solar structures. (iii) Non–solar changes in intensity that I will in general call here noise and that might also produce power. I already mentioned one such source in Sect. 3.1. Aschwanden et al. (2000) give a detailed discussion of errors in TRACE data.

The following statistical tests are performed to estimate the reliability of the peaks that one can find in the power spectra.

3.8.1. Randomisation test

To get an approximation of the influence of noise in the power spectra and to have an estimate of the significance of their peaks, I performed a randomisation test. The aim of this test is to find how significant the peak amplitude of a periodic signal is within a sequence of data points that also contains noise. Note that it is a purely statistical method so one still has to consider if the periodicities one finds are of solar origin or not (this is also true for the other tests described below). The randomisation test has successfully been applied to various problems in stellar physics: Linnell Nemec & Nemec (1985) used to obtain the statistical significance of the identification of secondary pulsations in Cepheids and RR Lyrae variable stars. It is also widely implemented in the search for periodic signals from other stars, e.g. to look for a planet in the radial velocity data of ϵ Eri (Hatzes et al. 2000), to study the X–ray variation of AB Dor (Kürster et al. 1997) or to search for brown dwarfs around solar–like stars (Murdoch et al. 1993). O'Shea et al. (2001, 2002a,b) have used it to reliably determine oscillations in sunspot umbrae. This test has the advantage that it is parameter free, which means that it does not rely on any assumptions about the distribution of the noise. It also can be used in connection with various kinds of periodicity finding algorithms (e.g. a wavelet analysis is used in O'Shea et al. 2001, 2002a,b). More detailed descriptions of the method are given in Linnell Nemec & Nemec (1985) and O'Shea et al. (2001).

The method has been applied in the following way: the original measured time sequence S_1 of each single pixel is

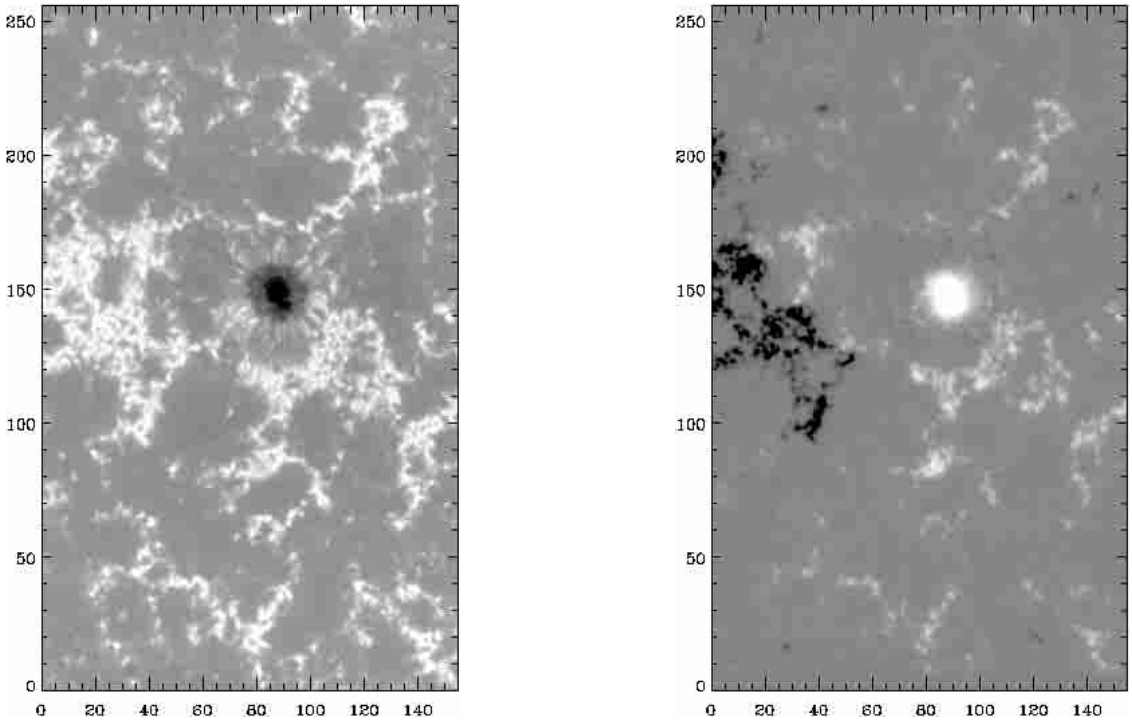

Fig. 2. Left: image of TRACE in the 1700 Å filter, brighter colour means higher intensity. It is a temporal average of the complete 4 h time sequence. The dark feature in the center of the field of view is the sunspot with umbra and penumbra. The bright patches are plage and network areas, in between is the internetwork. Right: snapshot of MDI magnetogram, the black and white represent the two magnetic polarities. The images show AR 9172, observed on September 29, 2000.

redistributed using a random generator. Then the power spectrum of this new sequence S_2 is calculated and compared with the power spectrum of S_1. This randomisation is repeated a number of times to get statistically significant results (see below). Then we count the fraction of times that a particular peak in the original power spectrum is higher than any peak in the randomised power spectra. This represents the probability p (in %) that the original peak is due to an actual periodicity in the data. In the following I set a probability limit of $p \geq 95\%$ (which means that power peaks with $p \geq 95\%$ are considered to be statistically significant).

A closer inspection of the power spectra (and other power spectra obtained within JOP097) reveals that the fluctuations seem to be frequency dependent. This means that the noise in the power spectra is also frequency dependent (non–white noise). To take this properly into account one would have to model all contributions to the power spectra (oscillatory and non–oscillatory solar and non solar effects) which is currently not possible. As the randomisation produces white noise out of the measured data it is valid only for white noise in the data.

Nevertheless, we can take this partly into account by applying the randomisation test iteratively: first, take the original sequence and look for significant power peaks as described above. In a second step those frequencies are filtered out (using a Fourier filter). Then the search for significant power peaks is repeated. In case one finds additional frequencies they are filtered out as well. The whole procedure is repeated until no significant frequencies are found anymore. After the final iteration all frequencies below the significance limit are set to zero.

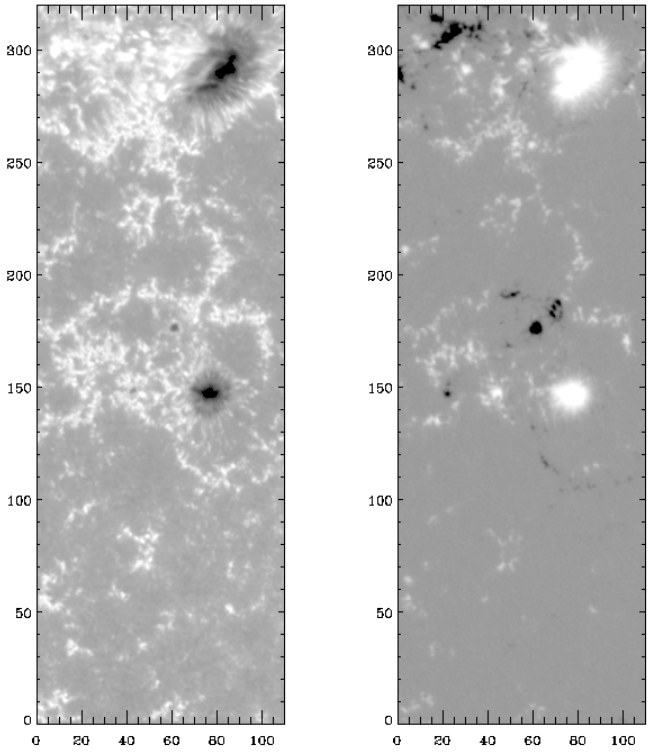

Fig. 3. The same as Fig. 2 but showing the TRACE 1700 Å temporally averaged image (left) and a snapshot MDI magnetogram (right) for AR 8693 and 8699 observed on September 13, 1999.

The biggest disadvantage of this method is that it is very time–consuming. It has to be done for each time sequence of

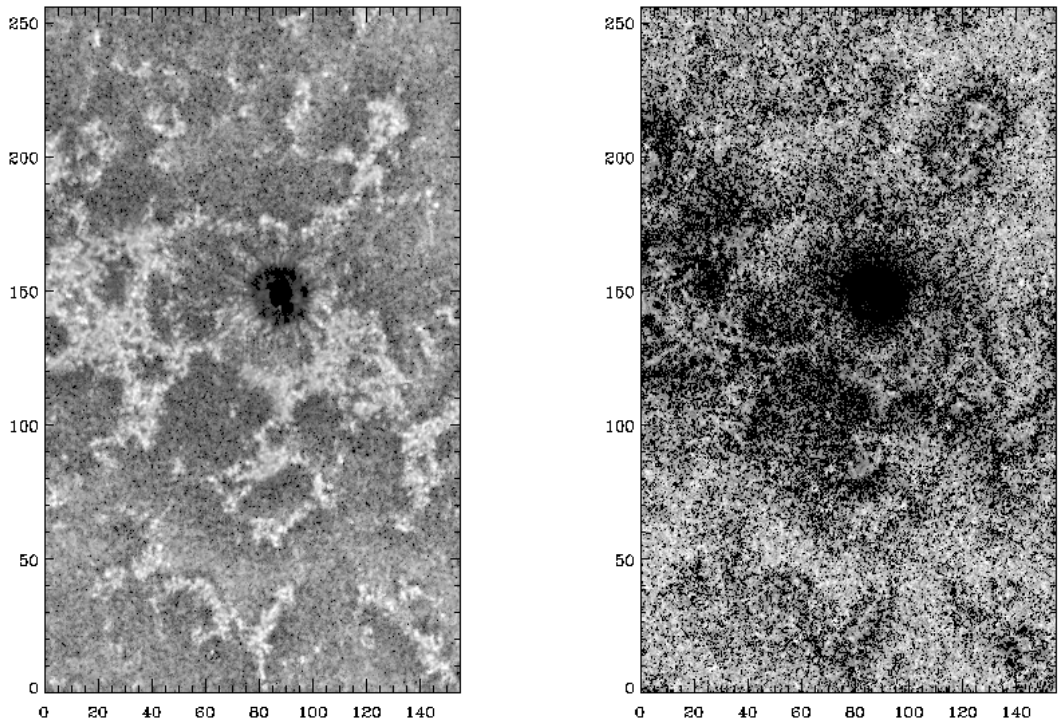

Fig. 4. Spatial distribution of intensity oscillatory power for the Sept. 2000 TRACE data (1700 Å channel). The left image shows the integrated power between 2.3–4.3 mHz (5 min range) and the right one between 5.5–7.5 mHz (2–3 min range). Only those power peaks that are statistically significant according to the randomisation test have been included, which means that all power with a probability less than 95% has been set to 0 and is thus not included when calculating the frequency bins (cf. Sect. 3.8.1). Dark areas have less power than bright ones.

the complete map separately and to get statistically reliable results one should carry out a sufficient number of permutations m of S_1. To test how large m should be I used the 1700 Å data from 2000 and set m = 100, 200, ..., 1000 and calculated the power maps for each value of m. Due to its statistical nature not all frequencies are found every time, but with increasing m the differences get smaller and smaller. So finally, m = 500 was chosen for the following analysis. To speed up the procedure all frequencies below 2 mHz are filtered out before starting the randomisation. These frequencies are of no interest for the current study and can also be influenced by the observing procedure (cf. Sect. 3.1).

3.8.2. Significance level according to Groth

Groth (1975) gives the significance of a power peak depending on the level of the (white) noise in the power spectra. We assume that all power above 7.5 mHz is due to noise and determine the average noise level to calculate the 99% significance level. To produce the final power maps we subtract this constant value from the power spectra. This method has frequently been used in solar oscillation studies (e.g. Balthasar et al. 1987; Solanki et al. 1996; Rüedi et al. 1998; Settele et al. 2002).

Figure 1 shows two examples of power spectra taken at a location in a network region (left) and an internetwork cell (right). The horizontal line gives the 99% significance level calculated according to Groth. The crosses on top of the figures indicate the frequencies where significant peaks were found by the randomisation test as described above (Sect. 3.8.1). The randomisation test is more rigorous in rejecting some peaks. E.g. a number of high frequency peaks (>6 mHz) in the internetwork spectrum lie slightly above the Groth level, but are not significant peaks in the randomisation test. It might well be that the randomisation test rejects peaks that still contain some oscillatory signal, on the other hand there is no doubt that the peaks that it finds significant represent an oscillation.

3.8.3. Spatial binning

Hill et al. (2001) have shown that simulating seeing on 2–d images can produce ring–like structures in power maps. Settele et al. (2002) also simulated image motion on their sunspot maps and found the largest artificial fluctuations of all measured parameters are at the location of the largest spatial derivatives. Although our data does not suffer from seeing, all numerical corrections have their limitations and small inaccuracies in the co–registration (as described in Sect. 3.6) may happen. Although the co–alignment of the data is probably better than one pixel I test this by summing up 2×2 and 3×3 pixels, thus decreasing the influence of co–alignment errors. Again, power spectra are calculated and the randomisation test as described above is applied to make the power maps.

3.9. Frequency binning

The final data set is a 3–dimensional data cube, with x and y, the spatial coordinates on the sun and frequency ν. To display these results as 2–dimensional figures I carry out a frequency

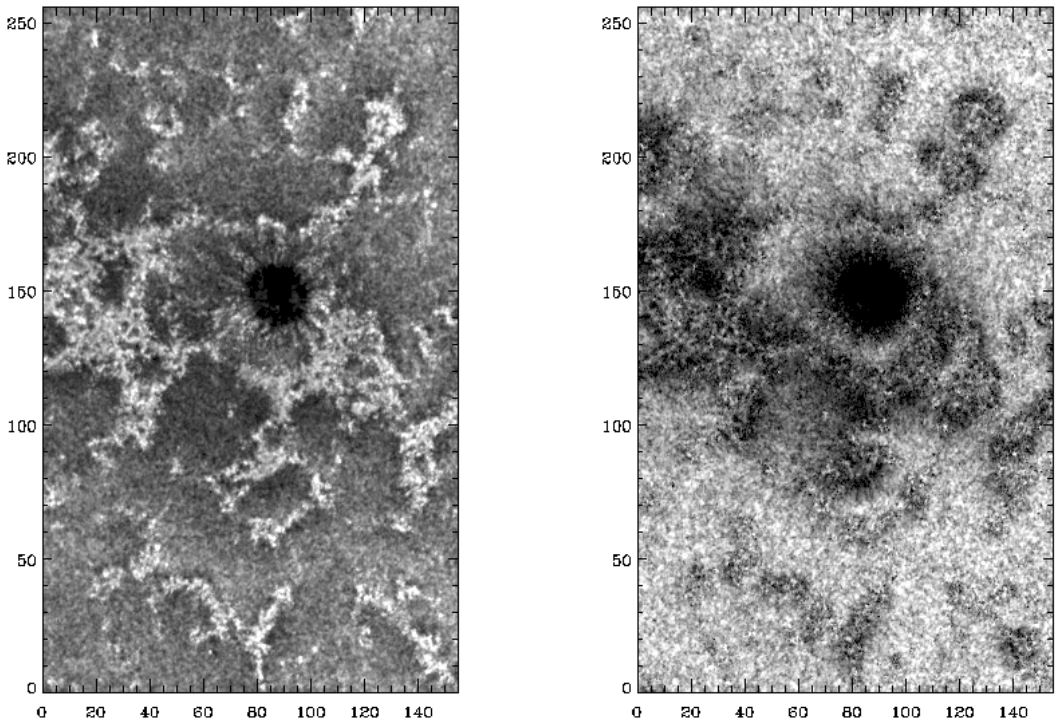

Fig. 5. Spatial distribution of intensity oscillatory power for the Sept. 2000 TRACE data (1700 Å channel). The left image shows the integrated power between 2.3–4.3 mHz (5 min range) and the right one between 5.5–7.5 mHz (2–3 min range). All power below a 99% significance level according to Groth (1975) has been subtracted before calculating the frequency bins (cf. Sect. 3.8.2). Dark areas have less power than bright ones.

binning. Two different frequency domains are of interest, one at 3.3 mHz (5 min) and the other one around 6 mHz (3 min periods). Thus, I integrate all power in the range of 2.3–4.3 mHz and 5.5–7.5 mHz. These maps are shown in Figs. 4–9.

4. Results

4.1. Topological context

The dynamics on the sun are closely related to the structure of the atmosphere. The solar magnetic field is the structuring agent.

Figure 2 (left) shows a temporal average of the 4 hours of co–aligned 1700 Å images (Sep. 2000) and next to it a single magnetogram taken by the Michelson Doppler Imager (MDI, Scherrer et al. 1995) on–board SoHO, giving the distribution of line–of–sight magnetic flux density of the same area (Fig. 2 right). AR 9172 contains a bipolar region with a moderately sized regular sunspot and surrounding plage area.

Figure 3 shows the same for the data from Sept. 1999. AR 8693 in the center of the FOV was the main target of the campaign on that day. A pore and plage of opposite polarity were north of the main spot. The AR on top of Fig. 3 was very active and showed a lot of brightenings during the 2 h sequence, which were visible in all filters (as can be seen in the movies on the web).

We can differentiate between three different magnetic domains within the FOV. (i) The dark structures in the 1700 Å images are sunspots and pores, with sunspot umbra and penumbra well recognizable. (ii) The bright structures around the spots are plage and further away from the AR is the bright chromospheric network. Immediately around the spot we can see radial spiky features. They are the signature of outward moving bright dots and can be identified in the magnetograms as moving magnetic features. For the spots, pores, plage and network we can find a one–to–one relation with the black and white features in the magnetogram. Note that MDI uses Ni I 6768 Å, which is formed around 100–200 km (Bruls 1993). Thus, the magnetic topology given here with an MDI filter magnetogram refers to the low photosphere.

All of these structures harbour strong (kG) magnetic fields in the photospheric layers of the solar atmosphere and differ primarily in size. Field strengths between 2000 and 4000 G are common in sunspot umbrae with a radially outward decrease. Observationally and semi–empirically determined intrinsic field strengths of the network are 1500 G at the $\tau = 1$ level (Stenflo 1973; Muglach & Solanki 1992). Various authors get the same values for the plage (Keller et al. 1990; Hasan et al. 1998; Bellot Rubio et al. 2000). Both plage and network can be considered as made of an assembly of small–scale magnetic elements, which all have very similar properties. The different flux density values in MDI are primarily due to different filling factors (plage is more densely populated with these fluxtubes than the network).

(iii) The dark cell like structures in the TRACE images are the internetwork cells. The internetwork (IN) is evenly grey in the magnetograms, which is partly due to the chosen contrast of the figures. Nevertheless, the flux values are very low (around zero), as the IN contains very little longitudinal magnetic flux. Thus, earlier works on chromospheric dynamics consider the

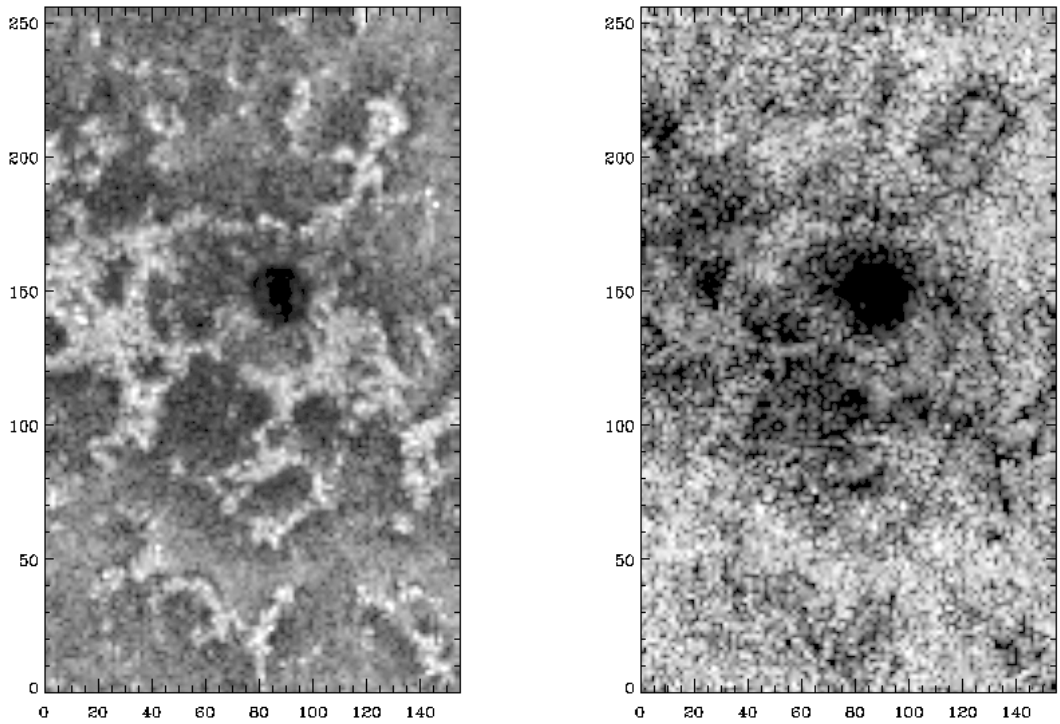

Fig. 6. Spatial distribution of intensity oscillatory power for the Sept. 2000 TRACE data (1700 Å channel). The left image shows the integrated power between 2.3–4.3 mHz (5 min range) and the right one between 5.5–7.5 mHz (2–3 min range). To increase the statistics I first sum up 3×3 pixels, then the iterative randomisation test has been applied before calculating the frequency bins (cf. Sect. 3.8.3). Dark areas have less power than bright ones.

IN as magnetic field free regions. This also makes wave propagation calculations much easier, as magnetic fields are usually not part of these calculations (e.g. Carlsson & Stein 1997). The true magnetic structure of the internetwork as well as its relation to internetwork dynamics are still under debate, see e.g. the recent papers of Lites et al. (1999) and Sivaraman et al. (2000) for diverging results on the magnetic nature of Ca II grains. Concerning internetwork field strengths, Lin (1995) used full Stokes vector polarimetry in the infrared and finds a broad distribution of field strengths peaking around 600 G. This confirms earlier findings from visible data (e.g. Keller et al. 1994).

Still weaker field values are obtained using Hanle effect diagnostics which give only a few Gauss for a turbulent (mixed polarity) magnetic field (e.g. Stenflo et al. 1998). A small scale mixed polarity topology is also supported by the observation and inversion of asymmetric and unusually shaped Stokes *V* profiles (e.g. Sigwarth 2001; Socas–Navarro & Sánchez Almeida 2002).

As can be seen in the magnetograms the ARs are bipolar, e.g. in Fig. 2 the inversion line of the two polarities runs diagonal to the left of the sunspot. Filaments were located along the inversion lines as could be seen in Hα images on the same day.

4.2. Power maps

Figures 4–6 show the result of the data reduction and the application of the various statistical tests. I use the data from the 1700 Å filter (of the 2000 campaign) as an example. Figure 4 left shows the spatial distribution of power in the 5 min frequency band, on the right is the map of 3 min power. Each image is linearly scaled, the brighter the region, the higher the power, black means that there is no power. The iterative randomisation test has been applied to the data, so only power peaks that are found to be statistically significant are included. Figure 5 shows the same as Fig. 4, but the 99% Groth level (cf. 3.8.2) has been subtracted from the raw power spectra. Figure 6 shows the analogous maps of the 3×3 pixels summed data (including the randomisation test after summing). Comparing the power distributions of Figs. 4–6 one can see that they all look very similar. The contrast in Fig. 5 is a bit higher than in Fig. 4. The decrease in spatial resolution is easily visible in Fig. 6, but the general large–scale pattern in the power distribution is still clearly present. Thus, all three tests give consistent results.

The sunspot displays several well–known features. The umbra is completely black in all maps which means that there is no significant power. This is an effect of the low count-rate that we have in the dark umbra at full spatial resolution. When summing up a larger number of pixels we find the signature of umbral oscillations in the 3 min range as demonstrated in Muglach & O'Shea (2001). These oscillations are well known from ground–based observations (see e.g. Lites 1992 for a review). They have also been observed in EUV spectra by other space instruments such as SUMER and CDS on–board SoHO (e.g. Brynildsen et al. 2002, see review by Staude 1999). In the penumbra one can see significant power in the 5 min range. There is also the signature of radially outward moving waves, which can be confirmed by displaying the sequence of images

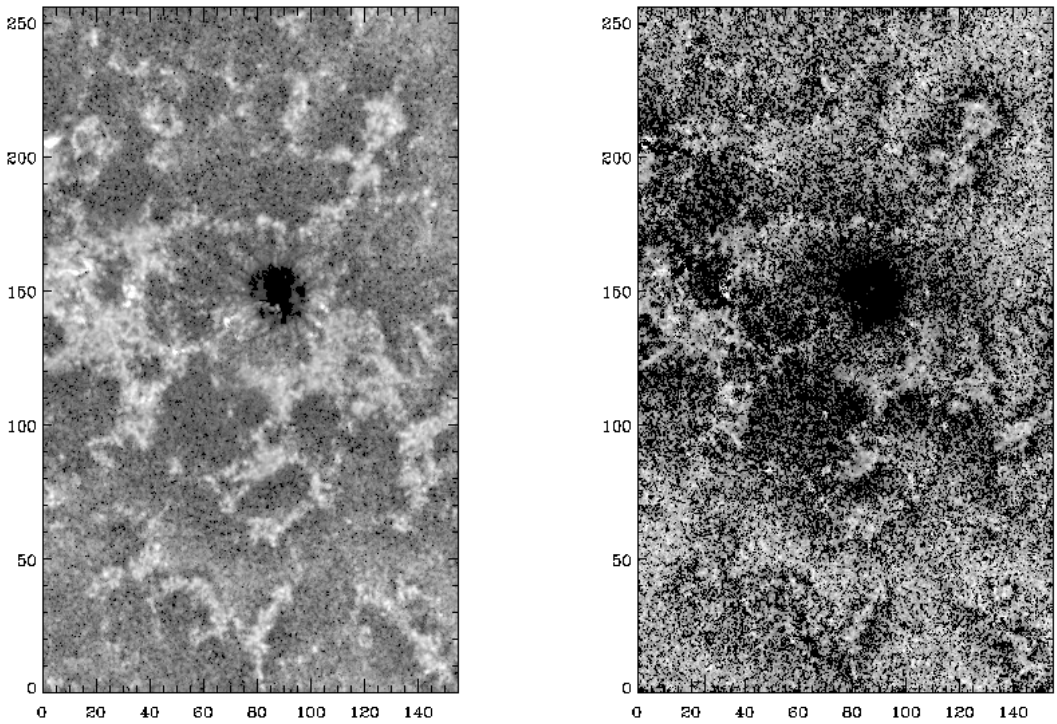

Fig. 7. Spatial distribution of intensity oscillatory power for the Sept. 2000 TRACE data (1600 Å channel). The left image shows the integrated power between 2.3–4.3 mHz (5 min range) and the right one between 5.5–7.5 mHz (2–3 min range). Only those power peaks have been included that are statistically significant according to the randomisation test, which means that all power with a probability less than 95% has been set to 0 and is thus not included when calculating the frequency bins (cf. Sect. 3.8.1). Dark areas have less power than bright ones.

as a movie. Georgakilas et al. (2002) have analysed these waves in great detail and I refer the interested reader to this paper.

Outside the sunspot there is plage, network and internetwork. It is well known from ground–based observations of e.g. the Ca II K and H line that there is a distinct difference in wave frequencies between quiet sun network and internetwork: the network is dominated by oscillations with periods of 5 min and longer, while the internetwork displays additional power in the 3 min range (e.g. Rutten & Uitenbroek 1991). This is confirmed in Figs. 4–6. The brightest patches in the 5 min map can be found at the locations of the network and plage, when comparing Figs. 4–6 with Fig. 2. The nature of the network oscillations is still not known, although the fact that the network (and plage) consists of small–scale strong–field magnetic elements hints at a connection to these fluxtubes. The 3 min internetwork oscillations (as observed in the Ca II H line) have been successfully reproduced by acoustic waves that travel into the chromosphere and form shocks in the higher layers (Carlsson & Stein 1997).

Figures 4–6 show another interesting and new feature, especially in the 3 min map: in the surroundings of the spot, plage and network the 3 min power is considerably lower than in the internetwork away from the AR. This is quite a large–scale effect and produces a dark area around the AR. The low field region in the plage around $x = 30''$ and $y = 150''$ almost completely disappears in the 3 min maps, which means that there is hardly any significant power. When comparing this region with the magnetogram one can see that it lies exactly at the magnetic neutral line (between the black and white of the two polarities). The same is true for a large internetwork cell centered at $x = 60''$ and $y = 100''$, which shows a gradient of power radially away from the sunspot. The network regions further away from the spot show a darkening immediately around them as well. This darkening is also slightly recognizable in the 5 min maps but is quite pronounced in the 3 min maps. None of the AR studies listed in the introduction mention such an effect, so this is a new finding in large–scale AR dynamics. Nevertheless, first hints of this can also be found around quiet sun network structures and are mentioned by Judge et al. (2001) and Krijger et al. (2001), which is in agreement with my own quiet sun data. McIntosh et al. (2001) argue that some of the observations of Judge et al. (2001) and others can be explained by differences in the magnetic field topology which can influence the oscillation pattern found in the higher atmosphere. This will be discussed in more detail in a follow-up paper (Muglach & Hofmann, in preparation). Figures 7 and 8 show the power maps of the 1600 Å and 1550 Å filters respectively. The same patterns can be found in them as well. Additionally, an increased influence of transition region dynamics is visible with increased formation temperature (or smaller wavelength of the filter) as bright horizontal structures in the plage region and in the penumbra of the spot (primarily seen in the 5 min maps). These are due to short–term brightenings typical for TR dynamics. Finally, Fig. 9 summarizes the results of the data from 1999, 5 min maps are on top, 3 min maps at the bottom, 1700 Å, 1600 Å and 1550 Å from left to right. The resulting power distribution is completely consistent with the results described above. As mentioned earlier AR 8699 at

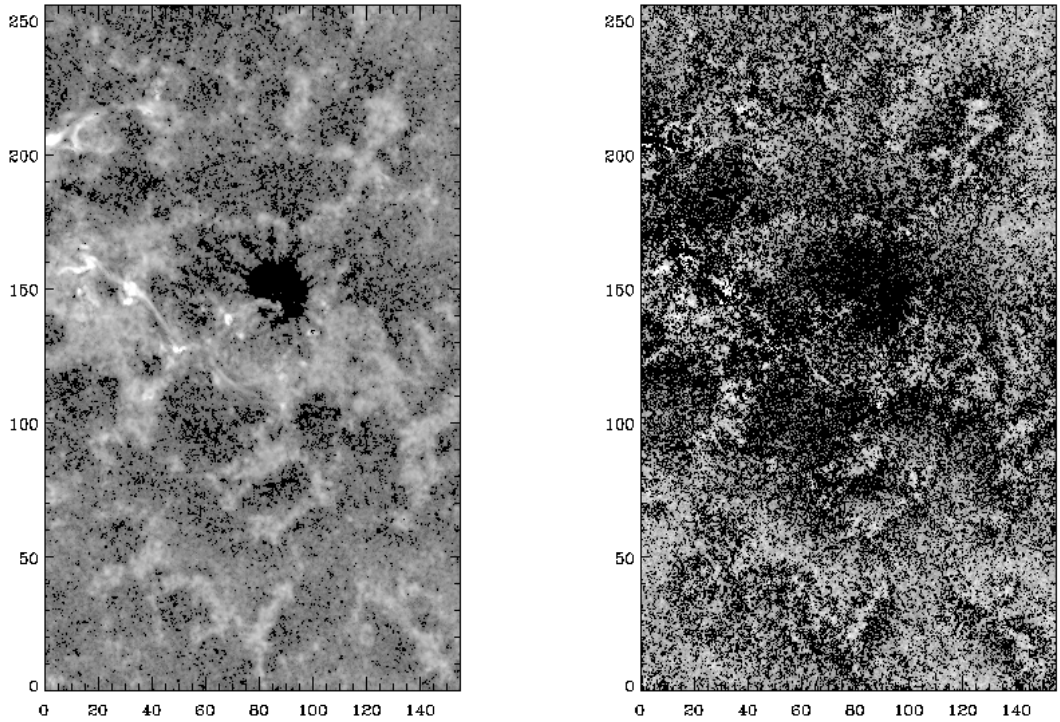

Fig. 8. Spatial distribution of intensity oscillatory power for the Sept. 2000 TRACE data (1550 Å channel). The left image shows the integrated power between 2.3–4.3 mHz (5 min range) and the right one between 5.5–7.5 mHz (2–3 min range). Only those power peaks have been included that are statistically significant according to the randomisation test, which means that all power with a probability less than 95% has been set to 0 and is thus not included when calculating the frequency bins (cf. Sect. 3.8.1). Dark areas have less power than bright ones.

the top of the FOV was very active during the observing time, which can be seen as white areas in the power maps, getting more extended the higher the formation temperature.

5. Discussion

I would like to suggest the following scenario to explain the observation of low power areas around strong magnetic field regions: at the lower photospheric level there are acoustic waves in the internetwork (the global *p*–modes). These waves can travel upward, especially those at frequencies above the acoustic cut-off frequency of 5.5 mHz. In higher layers they interact with the expanding magnetic field of the sunspot and the magnetic elements that make up the network and plage. The increase of the diameter of magnetic fluxtubes is a standard feature of all fluxtube models. As the fluxtubes expand with height, their field lines get more and more inclined until they either become horizontal or encounter field lines from other fluxtubes. Thus, they form a so-called magnetic canopy. As mentioned in the beginning the TRACE filtergrams at 1700 Å probe the quiet solar atmosphere at a height of about $h = 400$–500 km. If the inclined or horizontal magnetic field is below this height then the acoustic waves interact with the canopy boundary before they reach the height we can probe. This could be e.g. the case in the low flux region within the plage area around $x = 30''$ and $y = 150''$, which is supported by the fact that this is also the location of the magnetic neutral line. Considering the expansion rate of a large fluxtube (sunspot) and a small one (magnetic element) then one finds that it scales with size and thus the effect is a lot more extended in the sunspot than in the network.

What might be the nature of the interaction of the acoustic waves with the overlying magnetic field? Theoretical studies by Zhugzhda & Dzhalilov (1984a,b). find that the waves can be reflected or there can be a mode conversion (a purely acoustic wave couples to the magnetic field and progresses as a magneto–acoustic wave along the field lines). If this interaction happens below the observed height, then in both cases we would get less acoustic power, which is what is actually observed. First numerical calculations have recently been carried out by Rosenthal et al. (2002) for more complex magnetic field configurations but still under very idealised physical conditions.

Comparing our observations with previous 2–d investigations of chromospheric dynamics they seem to contradict observed Ca II K power halos (Braun et al. 1992; Toner & LaBonte 1993; Thomas & Stanchfield 2000). These power enhancements were also investigated using photospheric data from ground and from MDI (Thomas & Stanchfield 2000; Brown et al. 1992; Hindman & Brown 1998; Donea et al. 2000; Jain 2001; Jain & Haber 2002). In this case the intensity power maps show neither enhancement nor darkening around the sunspot. Nevertheless, in power maps of Doppler velocity they also find an enhancement of 3 min power.

This leads to a possible explanation of Ca II K 3 min power halos, assuming power halos in velocity in the photosphere. Ca II K and H filtergrams may not be clean intensity diagnostics as the lines get Doppler shifted and may thus produce intensity changes. TRACE 1700 Å and 1600 Å are broad–band filters (200 Å) and thus, a clean intensity diagnostic. In detail

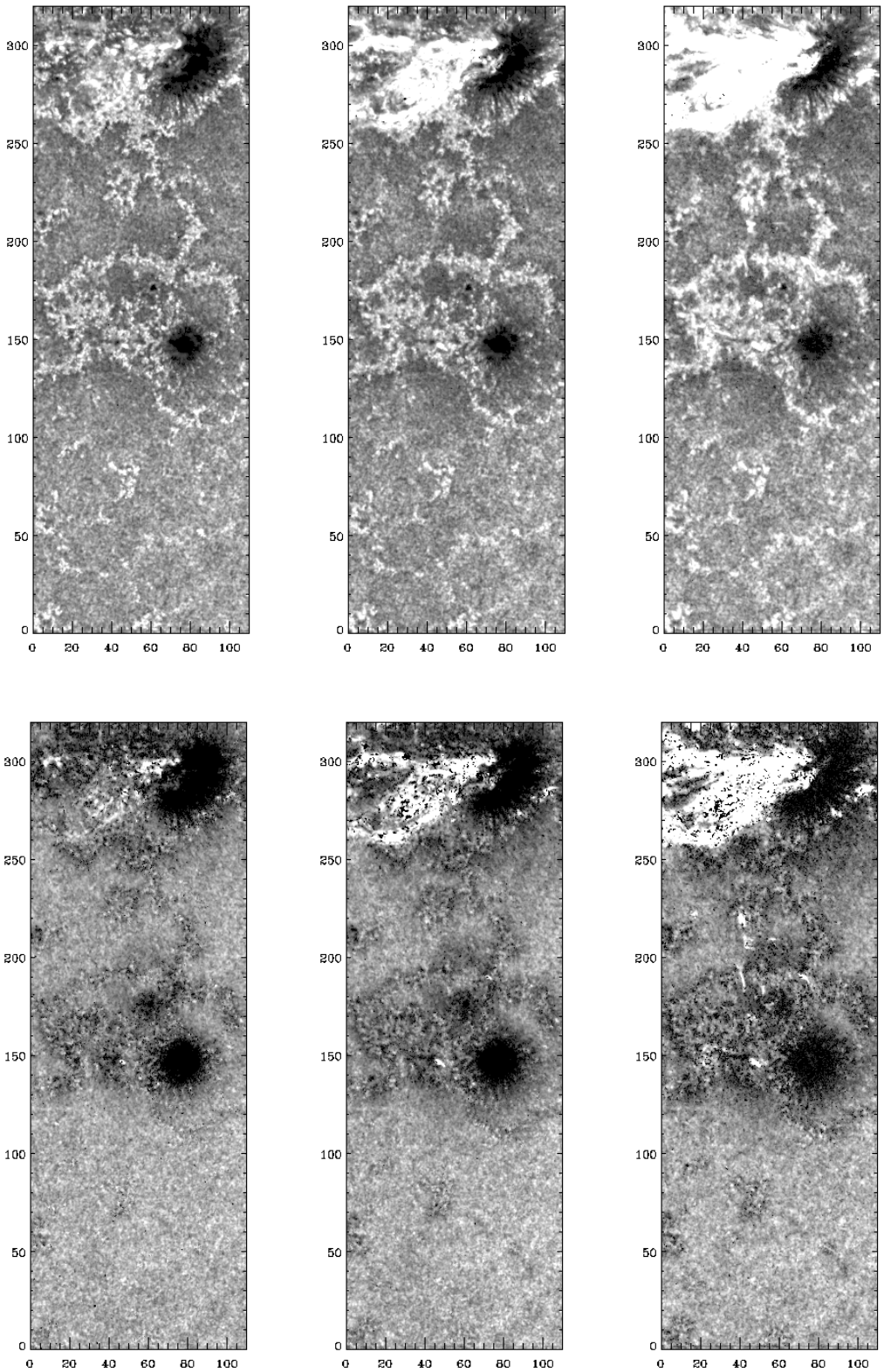

Fig. 9. Spatial distribution of intensity oscillatory power for the Sep. 1999 TRACE data in 1700 Å, 1600 Å and 1550 Å (from left to right). The top images show the integrated power between 2.3–4.3 mHz (5 min range) and the bottom ones between 5.5–7.5 mHz (2–3 min range). Only those power peaks have been included that are statistically significant according to the randomisation test, which means that all power with a probability less than 95% has been set to 0 and is thus not included when calculating the frequency bins (cf. Sect. 3.8.1). Dark areas have less power than bright ones.

the response of the Ca II K and H lines to a photospheric driver is non-linear (Carlsson & Stein 1997), thus, the enhanced velocity in the photosphere might also produce enhancement of the central core of the Ca II K line. In addition, the power halos in Braun et al. (1992) and Toner & LaBonte (1993) are very hard to compare directly with the power maps shown here due to the large difference of observing parameters and analysis. A possible solution of this puzzle would be a comparative study of Ca II K and TRACE UV power maps.

McIntosh & Judge (2001) concluded that a closed magnetic field structure is needed to explain the magnetic shadows of Judge et al. (2001). Note that one can find a decrease of 3 min power around all strong field structures, including uni-polar ones that do not have an opposite polarity nearby to form a low closed field. Either a weak opposite polarity is nearby that can not be detected or one does not need a nearby opposite polarity at all. The fact that we see the power decrease around all network/plage/spots indicates the latter. Nevertheless, in locations of two opposite polarities next to each other the effect is most pronounced. A more detailed discussion of the magnetic field configuration will be presented in a subsequent paper (Muglach & Hofmann 2003).

It has long been known that the solar magnetic field influences the solar oscillations. In this paper I have shown that this can also be turned around, namely, certain properties of the solar magnetic field can be determined by studying the dynamics.

6. Summary and outlook

In this paper I have presented an analysis of time sequences of filtergrams taken by TRACE at 1700 Å, 1600 Å and 1550 Å. A detailed description of the data reduction and the statistical analysis is given. The main result is the presence of low power areas around the ARs in the 3 min intensity power maps. This lack of power which is also present around well-developed network is interpreted as due to the interaction of the underlying acoustic wave field with the inclined magnetic field of the AR (either due to wave conversion or wave reflection).

The results of this work leave ample space to further investigate this topic and clarify some of the following items.

One possibility to verify the above interpretation is the calculation of the actual magnetic field topology via a magnetic field extrapolation. For the Sep. 2000 data MDI magnetograms are available and such calculations are currently in progress.

As we have time–sequencies of these MDI data, we can also produce low photospheric power maps (similar to other MDI studies of that kind) and can thus make a direct, one–to–one comparison of the power distributions.

These first two points are currently under investigation and will be the topic of a follow–up paper (Muglach & Hofmann 2003).

From an observational point of view it would also be desirable to make such a comparison with Ca II K images, because a simultaneous and co–spatial data set should be able to solve the puzzle of the Ca II K power halos.

In a next step the current TRACE data can be used to calculate phase and coherence spectra of the waves to see how the phase relations change due to the magnetic field.

One weakness of the interpretation presented in this article is the assumed formation height, which is only valid for an averaged quiet sun. One would need detailed calculations of the formation height of the TRACE filters, especially for magnetized atmospheres.

Realistic numerical modelling of the wave propagation with a measured magnetic field distribution as input (and comparing the output with the power maps) would be very desirable, especially to get a better idea of the details of the interaction of the magnetic field with the oscillations (wave conversion and reflection).

Finally, a completely different test could be performed: using full Stokes spectro-polarimetry one can derive the complete magnetic field vector. Thus the field structure is determined at the formation level of the spectral line that is used and can be compared with simultaneously observed TRACE power maps.

Acknowledgements. This research is part of the TMR–ESMN (European Solar Magnetometry Network) supported by the European Commission. I would like to thank the TRACE instrument team and planners for their support during the observing campaigns. Special thanks go to T. Tarbell for his help in optimizing the TRACE observing program. I would also like to thank the members of the AIP J. Staude, H. Balthasar and A. Hofmann for their support during my stay there and members of the ESMN B. Fleck, E. O'Shea, R. Rutten, J. Krijger and P. Sütterlin for discussions and for providing some of their software. The magnetograms in Figs. 2 and 3 are courtesy of SoHO/MDI consortium. SoHO is a project of international cooperation between ESA and NASA.

References

Aschwanden, M. J., Nightingale, R. W., Tarbell, T. D., & Wolfson, C. J. 2000, ApJ, 535, 1027
Balthasar, H., Küveler, G., & Wiehr, E. 1987, Sol. Phys., 112, 37
Balthasar, H., Collados, M., & Muglach, K. 2000a, Astron. Nachr., 321, 121
Balthasar, H., Collados, M., & Muglach, K. 2000b, Proc. of the SoHO 10/GONG 2000 Workshop, Tenerife, ESA SP–464, 163
Bellot Rubio, L. R., Ruiz Cobo, B., & Collados, M. 2000, ApJ, 535, 489
Bogdan, T. J. 2000, Sol. Phys., 192, 373
Braun, D. C., Lindsey, C., Fan, Y., & Jefferies, S. M. 1992, ApJ, 392, 739
Brown, T. M., Bogdan, T. J., Lites, B. W., & Thomas, J. H. 1992, ApJ, 394, L65
Bruls, J. H. M. 1993, A&A, 269, 509
Brynildsen, N., Maltby, P., Fredvik, T., & Kjeldseth-Moe, O. 2002, Sol. Phys., 207, 259
Carlsson, M., & Stein, R. F. 1997, ApJ, 481, 500
Donea, A.-C., Lindsey, C., & Braun, D. C. 2000, Sol. Phys., 192, 321
Georgakilas, A. A., Muglach, K., & Christopoulou, E. B. 2002, ApJ, 576, 561
Groth, E. J. 1975, ApJS, 29, 285
Handy, B., Acton, L. W., Kankelborg, C. C., et al. 1999, Sol. Phys., 187, 229
Hasan, S. S., Kneer, F., & Kalkofen, W. 1998, A&A, 332, 1064
Hatzes, A. P., Cochran, W. D., McArthur, B., et al. 2000, ApJ, 544, L145
Hill, F., Ladenkov, O., Ehgamberdiev, S., & Chou, D.-Y. 2001, Helio– and Asteroseismology at the Dawn of the Millenium, Proceedings of the SoHO 10/GONG 2000 Workshop, ESA SP–464, 219

Hindman, B. W., & Brown, T. M. 1998, ApJ, 504, 1029
Howard, R. F., Harvey, J. W., & Forgach, S. 1990, Sol. Phys., 130, 295
Jain, R., & Haber, D. 2002, A&A, 387, 1092
Jain, R. 2001, Proceedings of the INTAS Workshop on MHD waves in Astrophysical Plasmas, ed. J. L. Ballester, & B. Roberts, 111
Judge, P. G., Tarbell, T. D., & Wilhelm, K. 2001, ApJ, 554, 424
Keller, C. U., Steiner, O., Stenflo, J. O., & Solanki, S. K. 1990, A&A, 233, 583
Keller, C. U., Deubner, F.–L., Egger, U., Fleck, B., & Povel, H. P. 1994, 286, 626
Kneer, F., & von Uexküll, M. 1993, A&A, 274, 584
Krijger, J. M., Rutten, R. J., Lites, B. W., et al. 2001, A&A, 379, 1052
Kürster, M., Schmitt, J. H. M. M., Cutispoto, G., & Dennerl, K. 1997, A&A, 320, 831
Linnell Nemec, A. F., & Nemec, J. M. 1985, AJ, 90, 2317
Lites, B. W. 1992, in Sunspots: Theory and Observations, ed. J. H. Thomas, & N. O. Weiss, NATO-ASI Series 375, 261
Lites, B. W., Rutten, R. J., & Berger, T. E. 1999, ApJ, 517, 1013
Lin, H. 1995, ApJ, 446, 421
McIntosh, S., & Judge, P. G. 2001, ApJ, 561, 420
McIntosh, S., Bogdan, T. J., Cally, P. S., et al., ApJ, 548, L237
Muglach, K. 2002, Il Nuovo Cimento C, in press
Muglach, K., & Hofmann, A. 2003, A&A, in preparation
Muglach, K., & O'Shea, E. 2001, Proc. of the INTAS Workshop on MHD waves in Astrophysical Plasmas, ed. J. L. Ballester, & B. Roberts, 155
Muglach, K., & Solanki, S. K. 1992, A&A, 263, p. 301
Murdoch, K. A., Hearnshaw, J. B., & Clark, M. 1993, ApJ, 413, 349
O'Shea, E., Muglach, K., & Fleck, B. 2002a, 12th Workshop on Cool Stars, Stellar Systems and the Sun, in press
O'Shea, E., Muglach, K., & Fleck, B. 2002b, A&A, 387, 642
O'Shea, E., Banerjee, D., Doyle, J. G., Fleck, B., & Murtagh, F. 2001, A&A, 368, 1095
Rosenthal, C. S., Bogdan, T. J., Carlsson, M., et al. 2002, ApJ, 564, 508
Rutten, R. J. 1999, Third Advances in Solar Physics Euroconference: Magnetic Fields and Oscillations, ed. B. Schmieder, A. Hofmann, & J. Staude, ASP Conf. Ser., 184, 181
Rutten, R. J., & Uitenbroek, H. 1991, Sol. Phys., 134, 15
Scherrer, P. H., Bogart, R. S., Bush, R. I., et al. 1995, Sol. Phys., 162, 129
Settele, A., Sigwarth, M., & Muglach, K. 2002, A&A, 392, 1095
Rüedi, I., Solanki, S. K., Stenflo, J. O., Tarbell, T., & Scherrer, P. H. 1998, A&A, 335, L97
Sigwarth, M. 2001, ApJ, 563, 1031
Sivaraman, K. R., Gupta, S. S., Livingston, W. C., et al. 2000, A&A, 363, 279
Solanki, S. K., Livingston, W., Muglach, K., & Wallace, L. 1996, A&A, 315, 303
Socas–Navarro, H., & Sánchez Almeida, J. 2002, ApJ, 565, 1323
Staude, J. 1999, Third Advances in Solar Physics Euroconference: Magnetic Fields and Oscillations, ed. B. Schmieder, A. Hofmann, & J. Staude., ASP Conf. Ser., 184, 113
Stenflo, J. O. 1973, Sol. Phys., 32, 41
Stenflo, J. O., Keller, C. U., & Gandorfer, A. 1998, A&A, 329, 319
Thomas, J. H., & Stanchfield, D. C. H. 2000, ApJ, 537, 1086
Toner, C. G., & LaBonte, B. J. 1993, ApJ, 415, 847
Vernazza, J. E., Avrett, E. H., & Loeser, R. 1981, ApJS, 45, 635
Zhugzhda, Iu. D., & Dzhalilov, N. S. 1984a, A&A, 132, 45
Zhugzhda, Iu. D., & Dzhalilov, N. S. 1984b, A&A, 132, 52